symmetry

MDPI

Article

Shaking Table Tests on the Seismic Response of Symmetrically Integrated Underground Stations

Shi Ming *, Lianjin Tao and Zhigang Wang

Key Laboratory of Urban Security and Disaster Engineering of Education, Beijing University of Technology, Beijing 100124, China; ljtao@bjut.edu.cn (L.T.); zgwang@emails.bjut.edu.cn (Z.W.)
* Correspondence: mings@emails.bjut.edu.cn

Abstract: This paper focuses on the seismic response of symmetrical underground subway stations to seismic waves with varying frequencies and peak ground accelerations (PGAs), essential in light of growing urban underground transit systems. A 1/40 scale station model was subjected to seismic simulations using waves from the Wenchuan and Tangshan earthquakes and an artificial wave spanning 0.1 g to 0.5 g PGAs. Shaking table tests revealed that seismic impacts divide at PGA = 0.3 g; high-frequency waves affect structures more below this threshold, while low-frequency waves have more impact above it. The columns on the third basement level responded more to seismic activity, particularly at their base. The study recommends prioritizing the seismic design of these columns during station construction, especially in earthquake-prone zones. Understanding the dynamic effects of different frequencies and amplitudes is crucial for selecting and reinforcing materials and structural designs to enhance seismic resistance.

Keywords: different seismic waves; underground integrated subway station; shaking table test; acceleration response

Citation: Ming, S.; Tao, L.; Wang, Z. Shaking Table Tests on the Seismic Response of Symmetrically Integrated Underground Stations. *Symmetry* **2024**, *16*, 232. https://doi.org/10.3390/sym16020232

Academic Editor: Kamran Foroutan

Received: 20 January 2024
Revised: 6 February 2024
Accepted: 10 February 2024
Published: 14 February 2024

1. Introduction

With the rapid development of underground railway systems worldwide, subway stations play an irreplaceable role in urban transportation networks. However, earthquakes, as unpredictable natural disasters, pose a serious challenge to the safe operation of subway stations. The underground station in the center of Kobe, which was heavily damaged during the Great Hanshin earthquake on 17 January 1995, serves as a prime example. The earthquake caused significant damage to 25 central columns located near the Chuo Expressway side of the station, with columns 5 to 11 being the most severely affected. Therefore, conducting research on the seismic response of subway stations is of great significance for ensuring public safety and the sustainable development of urban transportation. In recent years, scholars conducted a series of studies on the seismic resistance of subway stations and achieved some results. Su Jian et al. [1] studied the seismic response of the Tennoji Station using numerical simulation. Zhuang Haiyang et al. [2–5] investigated the isolation performance of subway stations through numerical simulation. Wang Jianning et al. [6–8] studied the seismic performance of subway stations with different spans using numerical simulation. Yue Cuizhou et al. [9] conducted vibration table tests on station structures with reinforced central columns. Ma Chao et al. [10] analyzed the influence of soil mechanic parameters on the seismic performance of underground structures using numerical simulation. Chen Zhiyi et al. [11] conducted vibration table tests on multi-layer subway stations to study their seismic response, finding that in addition to horizontal shear deformation, rotational vibration also occurs in subway stations. Bao Xiaohua et al. [12] conducted numerical simulation studies on the interaction of multiple underground structures and found that pile foundations and upper structures have a significant impact on column shear forces in station structures. Li Ming et al. [13] proposed a simplified analysis method combining mode decomposition and response acceleration methods for the seismic design

of integrated subway station structures. Through comparison using traditional seismic calculation methods, they proved that the results of this simplified method tend to be on the safe side. Han Xuechuan et al. [14,15] analyzed the seismic response of integrated structures above and below ground using vibration table tests and numerical simulations. Yantao Li et al. [16] analyzed the interaction law between tunnels and adjacent structures on a shaking table. Yao A et al. [17] studied the seismic response and liquefaction mechanism of the tunnel in a layered liquefied site using vibration table tests. Ming S et al. [18] studied the seismic response of underground integrated stations with liquefied soil layers using vibration table tests. Tao Lianjin et al. [19,20] conducted comparative studies on the seismic response of overall cast-in-place subway stations and prefabricated assembly subway stations through vibration table tests. Chen Qiang et al. [21] conducted research on the seismic performance of the connection between subway stations and tunnels through numerical simulations and vibration table tests. Zhang Zhiming et al. [22] compared the similarities and differences in the seismic response between atrium-style subway stations and frame-type subway stations through vibration table tests.

In summary, scholars made significant research achievements in the seismic response of underground structures, including prefabricated subway stations, atrium-style subway stations, integrated subway stations with upper decks, subway stations with different spans, and seismic response studies of framed subway stations, seismic response studies of underground utility tunnels, and dynamic interaction between tunnels and adjacent above-ground structures. The main research methods used are numerical simulation and shaking table tests. Among them, numerical simulation has advantages such as safety, economy, and rich data, but the reliability of its calculation results may be questioned if there is a lack of corresponding experimental support. Shaking table tests can provide real dynamic loading while also allowing precise control of test conditions (vibration frequency, amplitude, duration) and intuitive observation of the model's failure mode.

Earthquakes have the characteristics of suddenness, complexity, and severity. Regarding the suddenness of earthquakes, we do not know what the next earthquake will be like. We can only infer whether the existing structures meet the seismic requirements based on the records of previous earthquakes. As for the complexity of earthquakes, the composition of seismic waves themselves is particularly complex, and we do not know what the spectrum characteristics of the next seismic wave will be like. In terms of the severity of earthquakes, the intensity of seismic waves cannot be predicted, and we do not know the amplitude of the next seismic wave. Based on the characteristics of earthquakes, this article designs a vibration table test for the seismic response of underground integrated stations, aiming to study the impact of seismic waves with different dominant frequencies and peak ground accelerations (PGA) on the seismic response of underground integrated stations. Next, this article will provide a detailed introduction to the design process of the vibration table test, the construction of the test model, the selection of input seismic waves, and the configuration of the data acquisition system. Through the analysis of the test results, this article will explore the influence of different dominant frequencies and peak ground accelerations (PGA) on the seismic performance of station structures, evaluate the safety performance of subway stations under extreme seismic actions, and propose corresponding suggestions.

2. Preparation for Testing

2.1. Background to the Test

This experiment is set in an integrated underground subway station. The integrated subway station consists of the main station structure with ancillary underground structures on both sides. The main station structure is a three-story, three-span standard subway station structure, and the ancillary underground structures on either side are two-story, two-span structures. The main station structure is interconnected with the ancillary underground structures on either side of the first underground floor. The structural form of the

integrated subway station is shown in Figure 1. The structure is symmetric, so only half of it is represented.

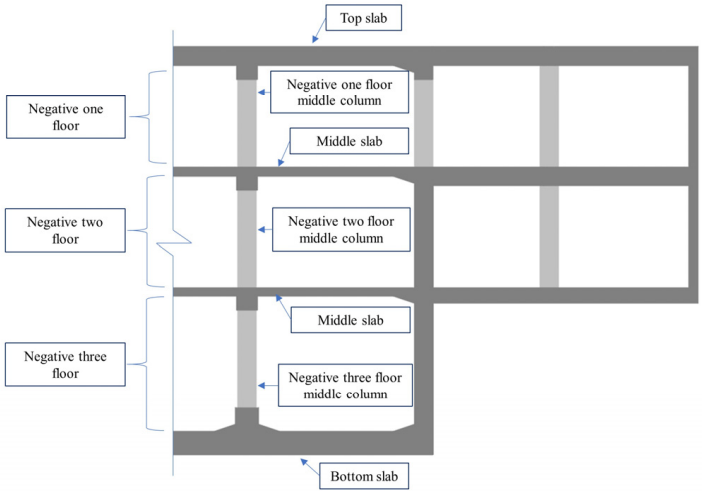

Figure 1. Structural form of underground integrated subway station.

2.2. Test Equipment and Similar Relationships

In the vibration table test of underground structures, laminated shear model boxes are widely used [23]. The shaking table and model box used in this test are shown in Figure 2. The technical parameters of the shaker are shown in Table 1. The model box is a laminar shear model box with a length of 2.5 m, a width of 1.2 m, and a height of 1.2 m. It consists of 14 layers of frames, with springs and dampers used to simulate the viscoelastic boundaries between each layer.

Shaking table Laminar shear box

Figure 2. Shaking table and model box.

Table 1. Technical parameters of the shaking table.

Name	Value	Unit
plane dimension	3 × 3	m
load capacity	10	t
weight	6	t
displacement	±127	mm
acceleration	±1	g
frequency	0.5~50	Hz

According to Buckingham's π theorem [24,25], length, modulus of elasticity, and acceleration are selected as the basic physical quantities for the design of the model structure similarity relationship. Considering the size of the model and the convenience of the sensor arrangement, the similarity relationship of each physical quantity is obtained, as shown in Table 2.

Table 2. Similarity relationships.

Typology	Physical Quantity	Relationships	Value
Geometrical features	Length l	S_l	1/40
	Moment of inertia I	$S_I = S_l^4$	3.9×10^{-7}
Material characterization	Density ρ	S_ρ	1
	Elastic modulus E	S_E	0.25
	Shear wave velocity of soil v	S_v	/
Dynamic properties	Force F	$S_F = S_\rho S_l^3 S_a$	1.6×10^{-5}
	Acceleration a	S_a	1
	Holding time t	$S_t = (S_l/S_a)^{0.5}$	0.158
	Dynamic response stress σ	$S_\sigma = S_l S_a S_\rho$	0.025

2.3. Model Structure Production

The physical and mechanical properties of micro-concrete and galvanized steel wire can simulate the corresponding properties of real concrete and rebar to a certain extent, making the structural analysis model more in line with actual engineering conditions. In the study of concrete materials and structures, the size effect is an important issue. Micro-concrete can simulate the size effect of real concrete structures on a small scale, facilitating scientific analysis and prediction [26]. Galvanized steel wire has good mechanical properties, approaching the strength level of some engineering rebars. Therefore, micro-concrete is used to simulate the concrete in underground structures, and galvanized steel wire is used to simulate the rebar in underground structures. Due to the complexity and irregular section of the station structure, the model structure is made using the method of bottom-up batch pouring through steps such as formwork support, rebar binding, micro-concrete pouring, and specimen curing. The production process is shown in Figure 3.

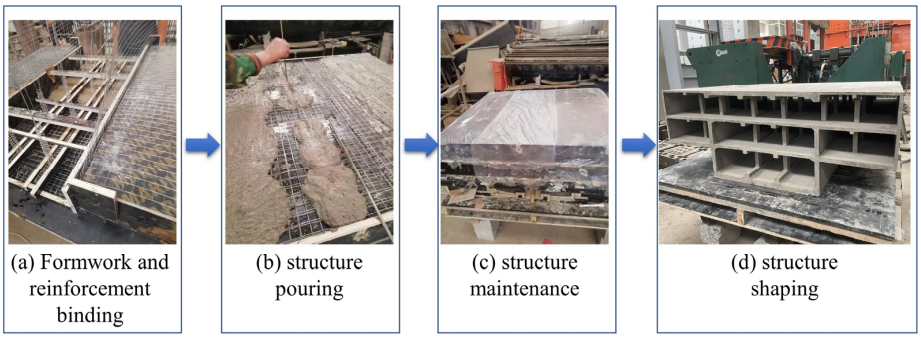

(a) Formwork and reinforcement binding (b) structure pouring (c) structure maintenance (d) structure shaping

Figure 3. Fabrication of the model structure.

Six sets of concrete specimens with side lengths of 70.7 mm × 70.7 mm × 70.7 mm were reserved while pouring the model to use in compressive strength tests (shown in Figure 4). The average cubic compressive strength of the test blocks was 7 MPa.

(a) Test block molding (b) Compressive test

Figure 4. Compressive strength test.

2.4. Preparation of Modeling Soil

The sandy soil used in this shaking table test came from an underground project site in Beijing. The sand was filled into the model box using a layered fill and tamping method. The process of model soil preparation was as follows (shown in Figure 5):

(1) Drying and sieving the sandy soil entering the test site;
(2) Attaching a soft ruler to the inside wall of the model box so that the amount of soil can be readily controlled while filling;
(3) Suspending the acceleration sensor in the designated position with a fishing line;
(4) Filling in and tamping in layers and sampling at appropriate locations using the ring knife method;
(5) When the sand was filled to a predetermined height (i.e., the location of the structure's base plate), the structure was lifted into position, and the sand continued to be loaded into the model box in layers until it reached the surface of the model;
(6) After the box was filled with sandy soil, the surface of the sandy soil was smoothed, the flatness of the surface was calibrated with a leveling ruler, and the sand was then covered with plastic sheeting to prevent moisture loss and consolidated under gravity for 24 h.

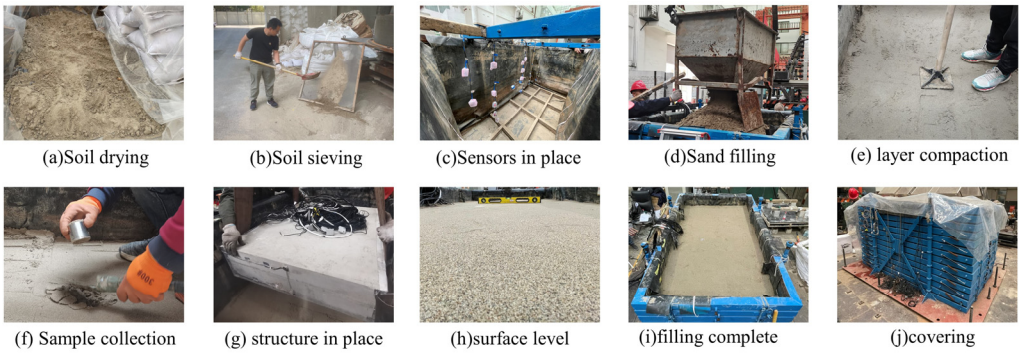

Figure 5. Modeled soil filling process.

During the experiment, soil samples were taken from appropriate positions in the model box. According to the standard for geotechnical testing method, the density of the sand used in the model test was measured to be $\rho = 1.7\ g/cm^3$, the moisture content was $\omega = 18\%$, and the internal friction angle was $\varphi = 33°$. From the grading analysis of the sandy soil (shown in Figure 6), the grain size grading curve (shown in Figure 7) was obtained. The curve shows that the coefficient of unevenness, $Cu < 5$, and the coefficient of curvature, Cc, of sandy soils range from 1 to 3.

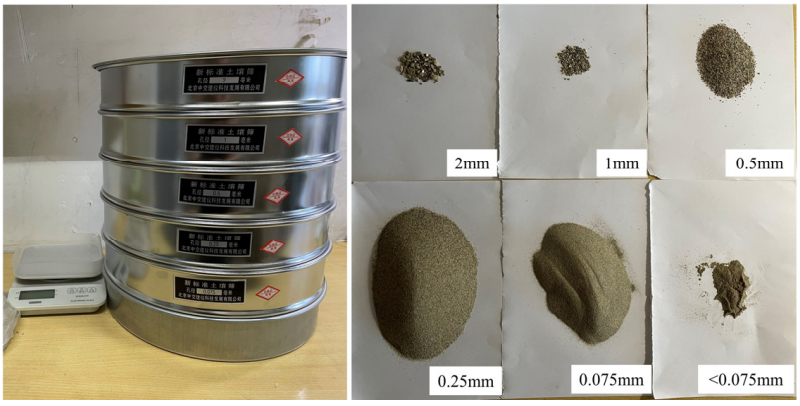

Figure 6. Sieve Test.

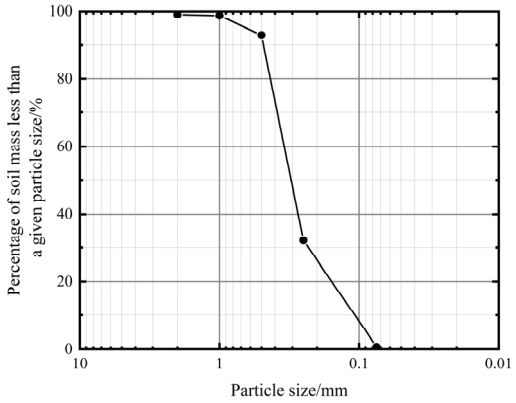

Figure 7. Particle grading curve.

2.5. Arrangement of Sensors

There are two components that need to be monitored in a shaking table test: one is the seismic response of the modeled soil, and the other is the seismic response of the underground structure. In the model soil, acceleration sensors are arranged to obtain the acceleration response of the soil. In the underground structure, acceleration sensors are arranged to obtain the acceleration response of the structure, strain gauges are used to identify the strain pattern of the structure, and Earth pressure sensors are installed to record the soil–structure interaction. The sensor arrangement in the model and in the structure are shown in Figures 8 and 9, respectively, where A denotes the acceleration sensor, S denotes the strain gauge, and T denotes the Earth pressure sensor. The adopted accelerometer is uniaxial, with a frequency range of 0.35 Hz to 300 Hz, a full scale of 2 g, and a resolution of 0.000008 g; the employed earth pressure sensor has a range of 200 kPa, a diameter of 28 mm, and a thickness of 10 mm; the utilized strain gauge is the BX120-10AA type, resistance-based, with a 30 cm lead wire, and a resistance of 120 $\pm$ 0.5Ω.

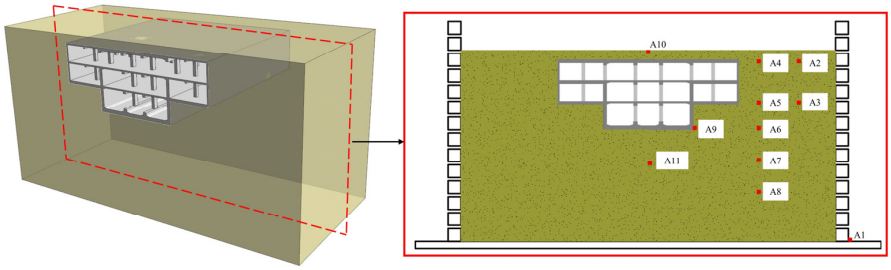

Figure 8. Acceleration sensor arrangement in model soil.

2.6. Selection of Seismic Wave and Loading Case Settings

The purpose of this experiment is to analyze the impact of seismic waves with different characteristics on the seismic response of underground integrated station structures. Therefore, seismic waves with different frequencies, amplitudes, and durations need to be considered. At the same time, referring to the research results of Han Xuechuan et al. [14,15], the regional characteristics of subway station structures should be comprehensively taken into account. So, the seismic waves selected for this test are the Ming−Shan wave, the Tangshan earthquake Beijing Hotel wave, and an artificial wave. The Ming-Shan wave was recorded during the 2008 Wenchuan earthquake, with an epicentral distance of 103 km, an original peak acceleration of 0.16 g, a holding time of 100 s, and a main frequency of 15.9 Hz. The Tangshan earthquake Beijing Hotel wave was recorded during the 1978 Tangshan earthquake, with an epicentral distance of 157 km, an original peak acceleration of 0.39 g, a holding time of 50 s, and a main frequency of 0.7 Hz. Finally, the artificial wave was taken from the seismic safety assessment report of a project in Beijing and had a peak acceleration of 0.26 g, a holding time of 40 s, and a main frequency of 5.2 Hz. The seismic

wave acceleration–time history curves, as well as the waves' Fourier spectra, are shown in Figure 10.

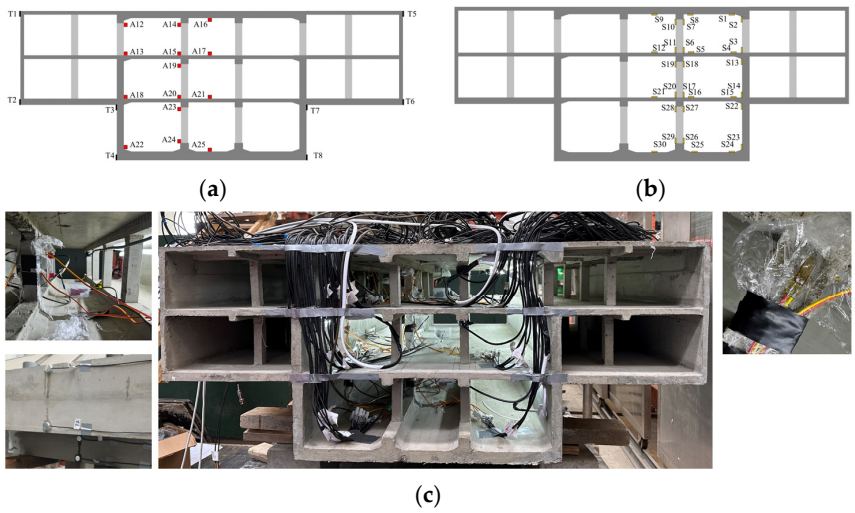

Figure 9. Sensor arrangement in the station structure. (**a**) Monitoring cross-section 1. (**b**) Monitoring cross-section 2. (**c**) Sensor arrangement.

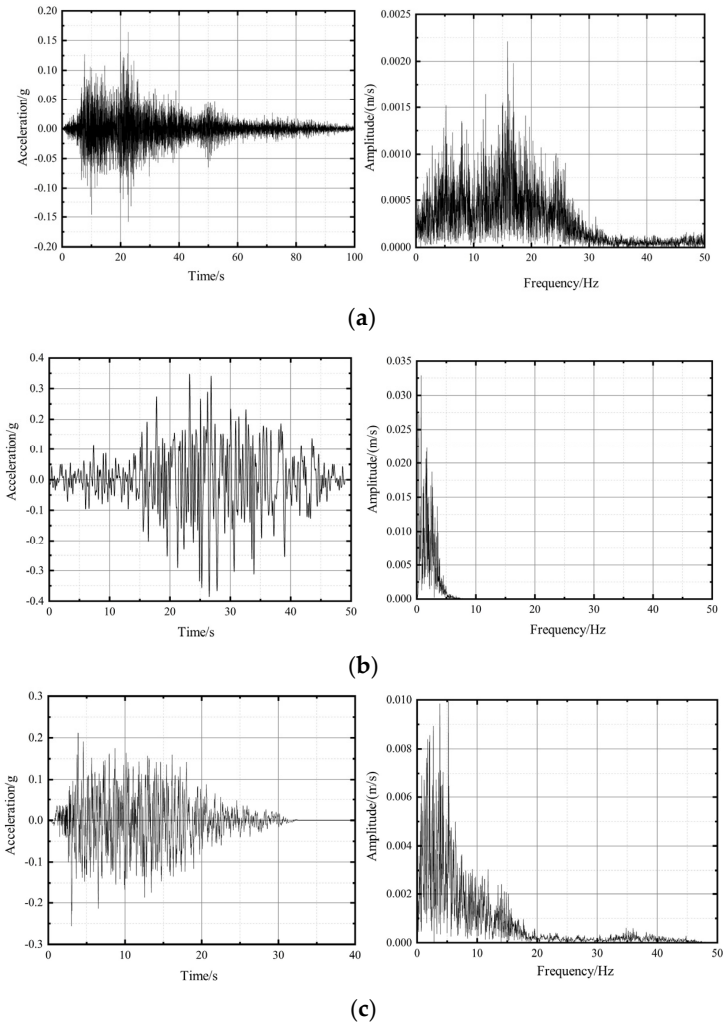

Figure 10. Time curves and Fourier spectra of seismic waves. (**a**) Ming−Shan wave; (**b**) Beijing Hotel wave; (**c**) artificial wave.

In the field of earthquake engineering and seismic wave data processing, baseline correction and normalization are two crucial steps. These processes contribute to the accuracy and reliability of seismic wave data during analysis and simulation.

(1) Baseline Correction

Seismic wave records may contain trend errors due to instrument inaccuracies or instability in data logging. These errors manifest as non-physical low-frequency components, potentially resulting in unrealistic drift in computed displacement or velocity time histories. The aim of baseline correction is to eliminate such non-physical drift, ensuring that the displacement or velocity of the seismic waves approaches zero over an extended period. This is accomplished by adjusting the baseline of the seismic wave record, that is, zero displacement line.

(2) Normalization

Normalization refers to the adjustment of the amplitude of seismic waves to a specific standard or range, usually for the purpose of comparison or to meet certain analysis requirements. The goal of normalization is to enable comparability in amplitude between different seismic waves or components or to adhere to specific amplitude constraints in experiments or analysis.

In the vibration table tests of underground structures, both baseline correction and normalization are critical data processing steps. They ensure that the seismic waveforms inputted into the tests are accurate and consistent.

Seismic waves underwent baseline correction and homogenization. The seismic waves were applied using a step-by-step loading method. The seismic wave loading scheme is shown in Table 3.

Table 3. Seismic wave loading settings.

Input Seismic Wave	Case	PGA/g
White noise	B−1	0.1
Ming-Shan wave	MS−1	0.1
Beijing Hotel wave	FD−1	0.1
Artificial wave	RG−1	0.1
White noise	B−2	0.1
Ming-Shan wave	MS−2	0.2
Beijing Hotel wave	FD−2	0.2
Artificial wave	RG−2	0.2
White noise	B−3	0.1
Ming-Shan wave	MS−3	0.3
Beijing Hotel wave	FD−3	0.3
Artificial wave	RG−3	0.3
White noise	B−4	0.1
Ming-Shan wave	MS−4	0.4
Beijing Hotel wave	FD−4	0.4
Artificial wave	RG−4	0.4
White noise	B−5	0.1
Ming-Shan wave	MS−5	0.5
Beijing Hotel wave	FD−5	0.5
Artificial wave	RG−5	0.5
White noise	B−6	0.1

3. Analysis of Test Results

3.1. Acceleration Response of Modeled Soil

The distribution of peak acceleration of modeled soil for different seismic waves as well as for different peak accelerations (PGA) is shown in Figure 11. When PGA $\leq$ 0.2 g, the acceleration response law of measuring points A4~A8 in the model soil is artificial wave > Ming−Shan wave > Beijing Hotel wave; When PGA = 0.3 g, the acceleration

response law of measuring points A5~A8 in the model soil is artificial wave > Beijing Hotel wave > Ming−Shan wave. When PGA > 0.4 g, the acceleration response law of measurement points A4 and A5 is artificial wave > Beijing Hotel wave > Ming−Shan wave, while the acceleration response law of measurement points A6~A8 is Beijing Hotel wave > artificial wave > Ming−Shan wave.

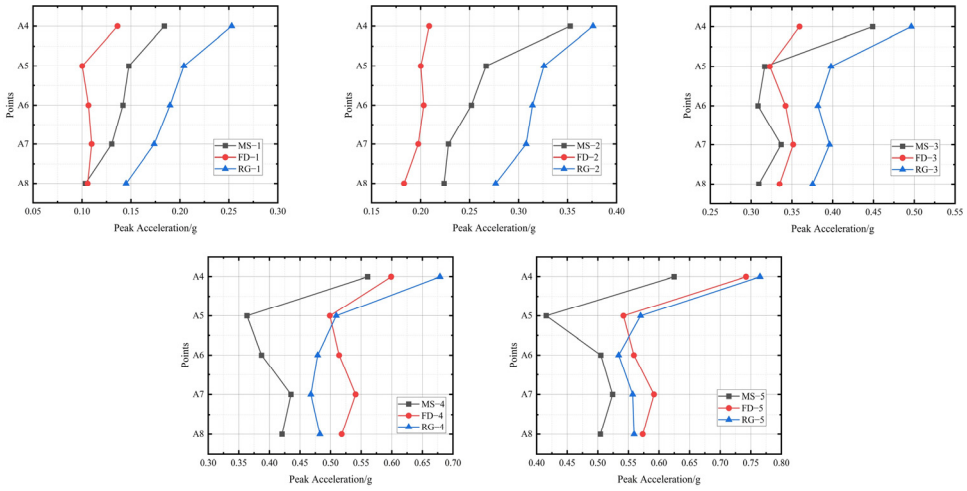

Figure 11. Distribution of peak acceleration of the model soil.

The acceleration amplification factors of the model soil under different seismic waves and different peak ground accelerations (PGA) are shown in Figure 12. When PGA $\leq$ 0.3 g, the pattern of acceleration amplification factors at measurement points A4 to A8 in the model soil is Ming−Shan wave > artificial wave > Beijing Hotel wave; when PGA = 0.4 g, under the Beijing Hotel wave, the acceleration amplification factors at measurement points A5 to A8 in the model soil are the greatest; when PGA > 0.4 g, under the Beijing Hotel wave, the acceleration amplification factors at measurement points A4 to A8 in the model soil are the highest.

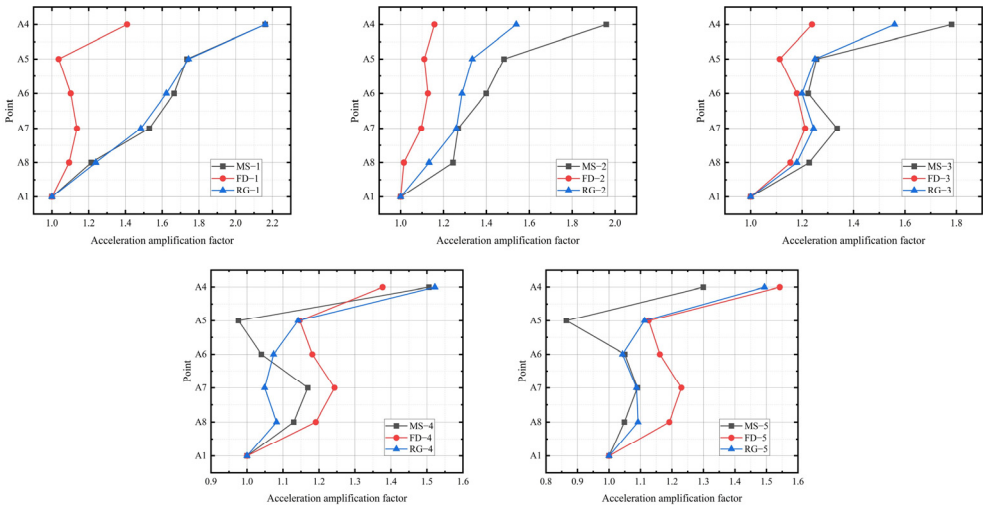

Figure 12. Acceleration amplification factor for model soil.

3.2. Acceleration Response of the Middle Column

The peak acceleration of the middle column of the first underground floor for different seismic waves, as well as for different peak accelerations (PGAs), is shown in Figure 13. In this case, measurement point A14 is located at the top of the middle column of the first underground floor, and measurement point A15 is located at the bottom of the middle

column of the first underground floor. When PGA $\leq$ 0.3 g, the acceleration response law of measurement points A14 and A15 is artificial wave > Ming−Shan wave > Beijing Hotel wave; when PGA > 0.3 g, the acceleration response law of measurement points A14 and A15 is artificial wave > Beijing Hotel wave > Ming−Shan wave.

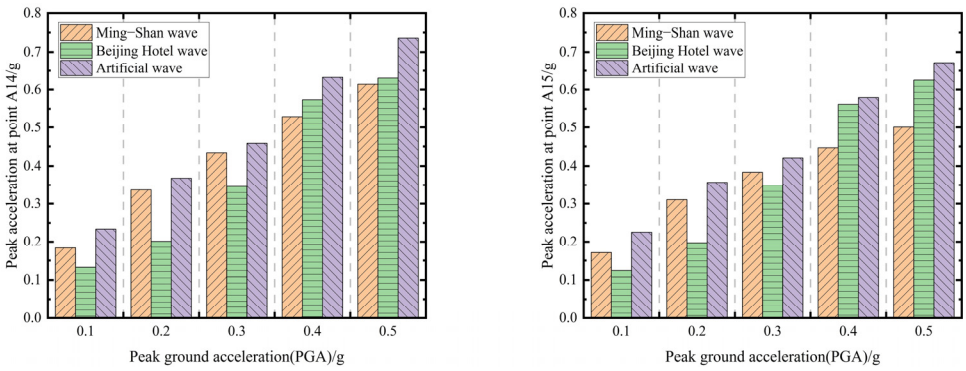

Figure 13. Peak acceleration of the middle column of the first underground floor.

Regardless of the seismic wave intensity, the acceleration response of the middle column of the first underground floor is always larger under the artificial wave than under the Ming−Shan or Beijing Hotel waves. When PGA > 0.3 g, the acceleration response of the middle column of the first underground floor is larger under the action of the Beijing Hotel wave than that under the action of the Ming−Shan wave.

The peak acceleration of the middle column of the second underground floor under different seismic waves, as well as for different peak accelerations (PGAs), is shown in Figure 14. In this case, measurement point A19 is located at the top of the middle column of the second underground floor, and measurement point A20 is located at the bottom of the same column. When PGA < 0.3 g, the acceleration response law of measurement points A19 and A20 is artificial wave > Ming−Shan wave > Beijing Hotel wave. When PGA = 0.3 g, the acceleration response law of measurement point A19 is artificial wave > Ming−Shan wave > Beijing Hotel wave, while the acceleration response law of measurement point A20 is artificial wave > Beijing Hotel wave > Ming−Shan wave. When PGA > 0.3 g, the acceleration response law of measurement point A19 is artificial wave > Beijing Hotel wave > Ming−Shan wave, while the acceleration response law of measurement point A20 is Beijing Hotel wave > artificial wave > Ming−Shan wave.

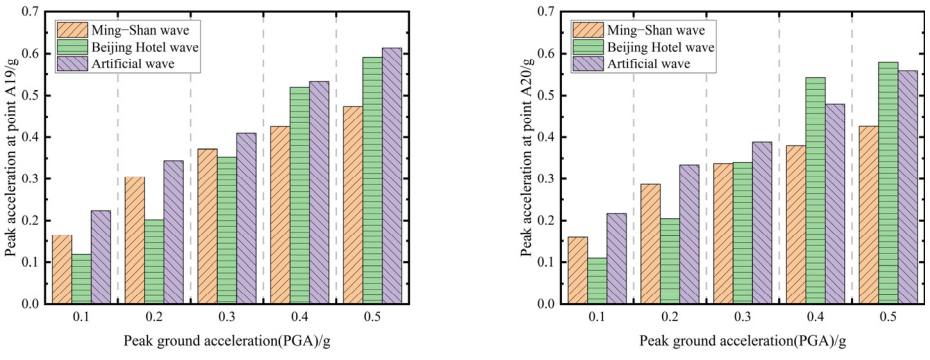

Figure 14. Peak acceleration of the middle column of the second underground floor.

The peak accelerations of the middle column of the third underground floor under different seismic waves, as well as different peak accelerations (PGAs), are shown in Figure 15. In this case, measurement point A23 is located at the top of the middle column of the third underground floor, and measurement point A24 is located at the bottom of the same column. When PGA < 0.3 g, the acceleration response law of measurement points A23

and A24 is artificial wave > Ming−Shan wave > Beijing Hotel wave. When PGA = 0.3 g, the acceleration response law of measuring points A23 and A24 is artificial wave > Beijing Hotel wave > Ming−Shan wave. When PGA > 0.3 g, the acceleration response law of measurement points A23 and A24 is Beijing Hotel wave > artificial wave > Ming−Shan wave.

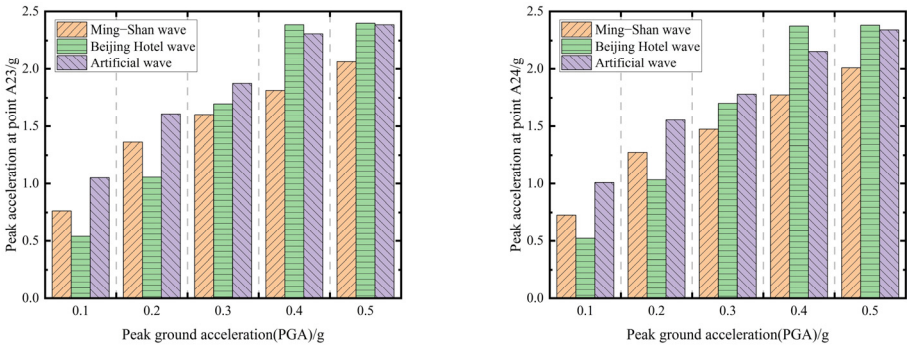

Figure 15. Peak acceleration of the middle column of the third underground floor.

Regardless of the seismic wave's intensity, the acceleration response of the middle column of the third underground floor is always greater under the artificial wave than under the Ming−Shan wave. When PGA < 0.3 g, the acceleration response of the middle column of the third underground floor is the smallest under the action of the Beijing Hotel wave. When PGA = 0.3 g, the acceleration response of the middle column of the third underground floor is smaller under the action of the Beijing Hotel wave than under the action of the artificial wave but larger than that under the action of the Ming−Shan wave. When PGA > 0.3 g, the acceleration response of the middle column of the third underground floor is the largest under the action of the Beijing Hotel wave.

3.3. Acceleration Response of Structural Slabs

The peak acceleration of the slab for different seismic waves, as well as for different peak accelerations (PGAs), is shown in Figure 16. In this case, measurement point A16 is located in the top slab, measurement point A17 is located in the middle slab of the first underground floor, measurement point A21 is located in the middle slab of the second underground floor, and measurement point A25 is located in the bottom slab. When PGA < 0.3 g, the acceleration response law of measurement points A16, A17, A21, and A25 is artificial wave > Ming−Shan wave > Beijing Hotel wave. When PGA = 0.3 g, the acceleration response law of measurement points A16 and A17 is artificial wave > Ming−Shan wave > Beijing Hotel wave, while the acceleration response law of measurement points A21 and A25 is artificial wave > Beijing Hotel wave > Ming−Shan wave. When PGA > 0.3 g, the acceleration response law of measurement points A16 and A17 is artificial wave > Beijing Hotel wave > Ming−Shan wave, while the acceleration response law of measurement points A21 and A25 is Beijing Hotel wave > artificial wave > Ming−Shan wave.

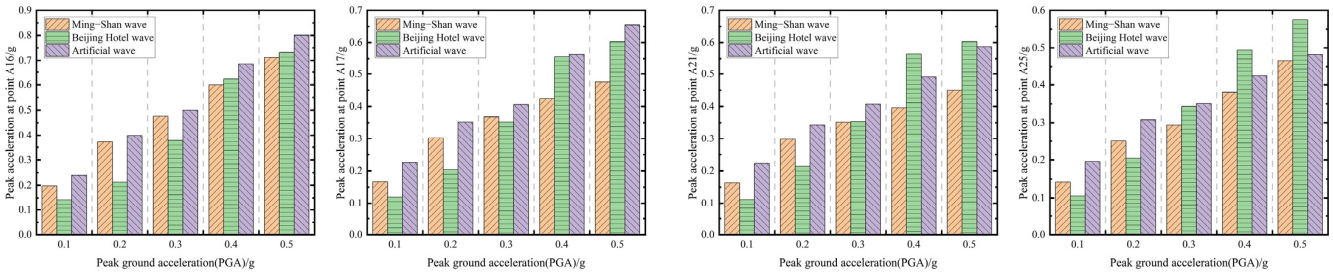

Figure 16. Peak acceleration of the slab.

When the PGA (peak ground acceleration) is 0.5 g, the acceleration–time history curve of the plate is shown in Figure 17. The acceleration–time history curves of the various measurement points are similar to the time history curve of the input seismic wave, indicating that the acceleration sensors are functioning properly, the data collection is accurate, and the data are reliable.

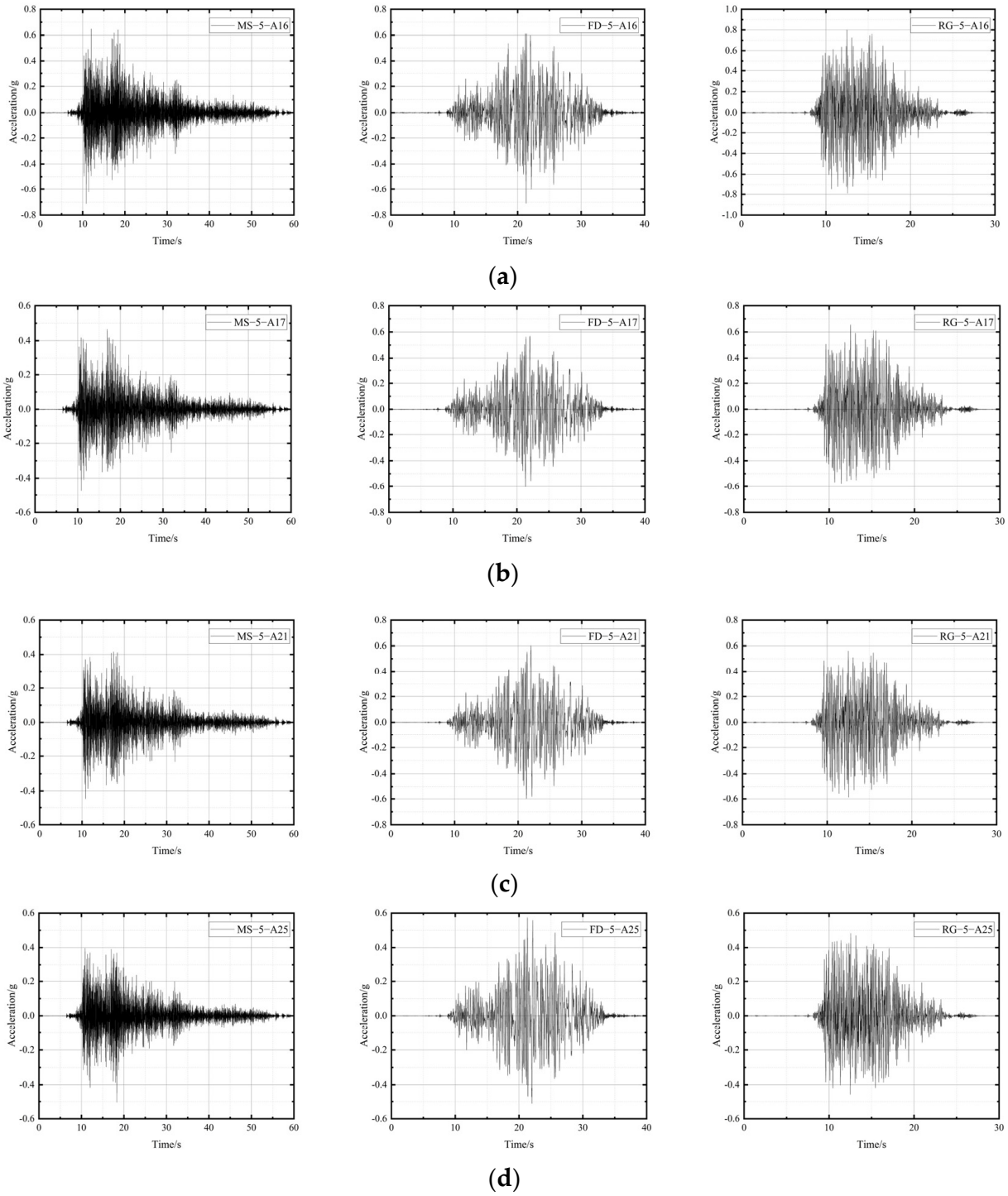

Figure 17. Acceleration−time history of slabs (PGA = 0.5 g). (**a**) Point A16; (**b**) Point A17; (**c**) Point A21; (**d**) Point A25.

3.4. Middle Column Strain Analysis

The strain amplitude of the middle column under different seismic waves with PGA = 0.5 g is shown in Table 4. The strain amplitude response law of measurement points S10, S11, S19, and S28 is artificial wave > Beijing Hotel wave > Ming−Shan wave. The strain amplitude response law of measurement points S20 and S29 is Beijing Hotel wave > artificial wave > Ming−Shan wave. The strain increment at the bottom of the middle column of the second underground floor and the bottom of the middle column of the third underground floor is slightly larger under the action of the Beijing Hotel wave than under the artificial wave. The strain increment response law of the middle column of the first underground floor, the top of the middle column of the second underground floor, and the top of the middle column of the third underground floor is artificial wave > Beijing Hotel wave > Ming−Shan wave. This indicates that the strain response of the middle column is larger under the action of the Beijing Hotel wave and the artificial wave, while the strain response of the middle column is smaller under the action of the Ming−Shan wave.

Table 4. Strain amplitude of the middle column under different seismic waves (με).

Position	Point	Case		
		MS−5	FD−5	RG−5
First underground floor, middle column	S10	37.23	65.92	73.25
	S11	23.19	30.52	40.90
Second underground floor, middle column	S19	8.55	25.64	35.40
	S20	61.65	115.36	111.70
Third underground floor, middle column	S28	6.10	18.92	32.35
	S29	217.91	369.90	356.47

3.5. Experimental Phenomena

The internal situation of the structure during the experiment is shown in Figure 18. The phenomena observed during the test are shown in Figure 19. The test resulted in surface cracking and the formation of cracks running along both sides of the structure, as shown in Figure 19a; the width of the cracks was 5 mm, as shown in Figure 19b. The test also resulted in damage to the soil immediately on either side of the structure to an extent of 60 mm, as shown in Figure 19c. Finally, the test resulted in soil subsidence on both sides of the structure, with a subsidence height of 13 mm, as shown in Figure 19d. The soil deformation is shown in Figure 19e.

Figure 18. Inside the structure.

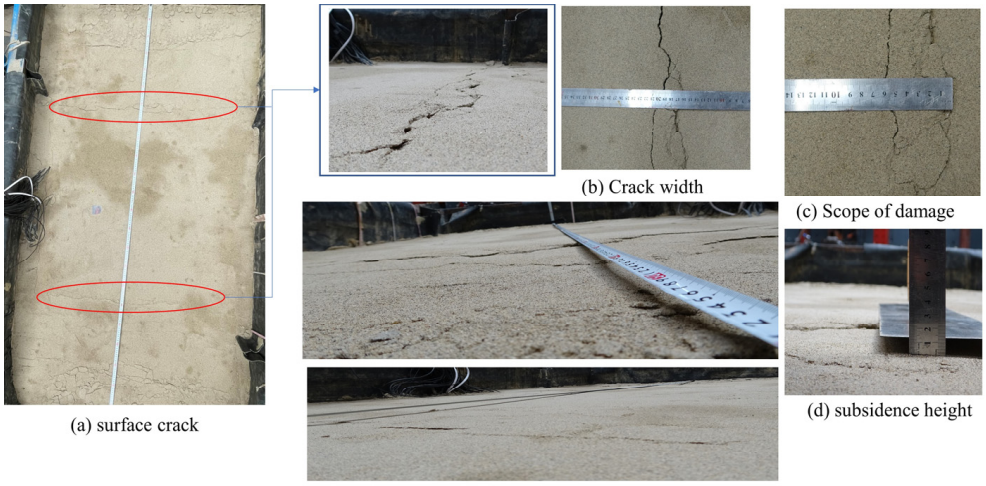

Figure 19. Soil phenomena of the test.

4. Discussion

This study, through a series of shake table experiments on an integrated underground station model, yielded several important findings concerning its seismic resistance. The experimental results not only quantitatively enhance our understanding of the responses of subway stations under seismic activity but also provide empirical evidence for quality seismic design.

In the experiment, seismic waves with different characteristics were applied, and it was observed that seismic waves of varying frequencies and amplitudes had different impacts on subway station structures. The structures were more sensitive to seismic waves within certain frequency ranges, which might be related to the structures' natural frequencies. Additionally, the resonance effect caused by seismic waves with a low-frequency dominance is particularly noteworthy, as it can lead to a more pronounced structural response. Therefore, in the design of subway stations, it is essential to implement specific earthquake-resistant designs that cater to the anticipated frequency characteristics of the seismic waves.

In the experiments, it was discovered that the presence of an integrated underground structure on both sides enhances the seismic resistance of the station structure. However, further research is still needed on the dynamic interaction between the soil layers and the integrated underground station structure to better understand and mitigate the impact of earthquakes on the entire underground construction.

It should be noted that there are certain limitations to shake table tests. Due to constraints in scale and cost, the test models are unable to fully replicate the complexity of actual subway stations. Furthermore, differences in the physical properties between model materials and real materials may affect the accuracy of the test results. Future research should consider more precise simulation methods or combine numerical simulations with actual survey data to obtain more convincing research outcomes.

In conclusion, the results of the shake table tests are of significant importance for the seismic design of underground integrated stations. Future research should delve further into the impact of different seismic motion parameters (including parameters of seismic waves and soil layers) on the seismic response of the underground integrated station structures, as well as how to incorporate this knowledge into the design to enhance their seismic safety. This is to ensure that the underground integrated station structures remain safe in operation during potential earthquakes that may occur in the future.

5. Conclusions

The research presented in this article conducted a systematic assessment of the seismic performance of an underground integrated subway station under the influence of earthquake waves with different frequencies and amplitudes through shake table tests. The experimental results revealed several important findings, providing crucial guidance for the seismic design of future subway stations.

(1) The seismic performance of a station structure is closely related to the frequency of earthquake waves. Low-frequency seismic waves result in larger structural responses. The Ming-Shan wave has a higher frequency, which has a smaller impact on the acceleration response of the central columns and structural slabs; artificial waves have a lower frequency, which has a greater impact on the acceleration response of the central columns and structural slabs; the Beijing Hotel wave has a very low frequency, and when the PGA > 0.3 g, its impact on the acceleration response of the central columns and structural slabs suddenly increases, especially affecting the acceleration response of the central columns and structural slabs on the negative third level the most.

(2) The impact of seismic waves of different magnitudes on subway stations is also significantly distinct. Under the influence of small-magnitude seismic waves, the station structure exhibits good elastic behavior. In contrast, under the influence of large-magnitude seismic waves, the structure may exhibit inelastic behavior and permanent deformation. This requires us to consider the potential risks of major seismic events in the design process.

(3) One significant characteristic of an integrated underground subway station is its "integrated" design, which allows for the effective dispersion of energy under the impact of seismic waves. As a result, since there are subsidiary underground structures on both sides of the station, the horizontal stiffness of the station structure at the first and second basement levels is greater than that of the third basement level. This leads to a much lower acceleration response in the central columns at the first and second basement levels compared to those at the third basement level. Therefore, in practical engineering applications, detailed dynamic analysis is required to optimize structural design and reduce the negative impact of stiffness differences on the earthquake resistance of the structure.

In summary, the shake table experiments conducted in this study provided valuable data and insights for understanding the dynamic response of integrated underground subway stations under the effects of seismic waves with varying frequencies and amplitudes. Based on these findings, it is recommended that future seismic designs should fully consider the impact of the frequency characteristics and amplitudes of seismic waves on the structural performance of subway stations. Moreover, despite the fact that shake table experiments can offer strong experimental support for seismic design, they still have certain limitations, including the differences between model materials and actual conditions and restrictions on model size, among other issues. Therefore, future research should combine a more diverse array of experimental methods and field investigation data to arrive at more comprehensive conclusions. Lastly, it is suggested that future studies should further consider the effects of soil–structure interaction under different seismic waves, as well as the impact of more complex underground structures on the propagation of seismic waves, in order to enhance the level of seismic design for underground structures.

Author Contributions: Conceptualization, S.M. and L.T.; methodology, L.T.; validation, S.M., L.T. and Z.W.; formal analysis, S.M.; investigation, S.M.; resources, S.M.; data curation, S.M.; writing—original draft preparation, S.M.; writing—review and editing, S.M.; visualization, Z.W.; supervision, L.T.; project administration, L.T.; funding acquisition, L.T. All authors have read and agreed to the published version of the manuscript.

Funding: This research was funded by [National Natural Science Foundation of China] grant number [42072308]. The APC was funded by [42072308].

Data Availability Statement: Data are contained within the present article.

Conflicts of Interest: The authors declare no conflict of interest.

References

1. Su, J.; Li, D.; Xu, M.; Cui, C.; Zhao, J. Seismic Response Analysis of Cross Transfer Subway Station. *J. Shenyang Jianzhu Univ. (Nat. Sci.)* **2023**, *39*, 820–827. (In Chinese)
2. Zhang, G.; Zhuang, H.; Xu, Z.; Wang, J. Seismic performance of two-story and three-span underground subway station structure under different foundation isolation cases. *J. Vib. Shock.* **2023**, *42*, 27–33+41. (In Chinese)
3. Zhuang, H.-Y.; Li, S.; Wang, W.; Jin, L.; Li, S.; Chen, G. Comparative analysis on seismic performance of two-story subway underground station structures with different isolating systems. *J. Vib. Eng.* **2023**, *36*, 379–388. (In Chinese)
4. Zhu, X.; Wang, W.; Zhuang, H. Seismic performance of the two-layer three-span subway underground station structure with lateral foundation backfill isolation layer. *Earthq. Eng. Eng. Dyn.* **2021**, *41*, 165–175. (In Chinese)
5. Chen, W.; Zhuang, H.; Li, S.; Chen, S. Seismic Performance of the Three-layer Three-span Subway Underground Station Structure with Seismic Isolation Bearings Fixed on the Top of Columns. *Technol. Earthq. Disaster Prev.* **2021**, *16*, 146–156. (In Chinese)
6. Wang, J.; Ma, G.; Dou, Y.; Zhuang, H.; Fu, J. Performance levels and evaluation method for seismic behaviors of a large-scale underground subway station with unequal-span frame. *J. Vib. Shock.* **2020**, *39*, 92–100. (In Chinese)
7. Wang, J.; Dou, Y.; Zhuang, H.; Fu, J.-S.; Ma, G.-W. Seismic responses of dynamic interaction system of soil-diaphragm wall-complicated unequal-span subway station. *Chin. J. Geotech. Eng.* **2019**, *41*, 1235–1243. (In Chinese)
8. Wang, J.; Zhang, G.; Zhuang, H.; Yang, J.; Li, C. Numerical investigation on seismic performance of a shallow buried underground structure with isolation devices. *Earthq. Res. Adv.* **2022**, *2*, 11–21. [CrossRef]
9. Yue, C.; Zheng, Y.; Deng, S. Shaking Table Test Study on Seismic Performance Improvement for Underground Structures with Middle Column Enhancement. *J. Earthq. Tsunami* **2019**, *13*, 23. [CrossRef]
10. Ma, C.; Zhou, S.; Chi, J. Seismic performance analysis of underground structures based on random field model of soil mechanical parameters. *Earthq. Res. Adv.* **2022**, *2*, 100170. [CrossRef]
11. Chen, Z.; Huang, P.; Chen, W. Seismic response characteristics of multi-story subway station through shaking table test. *Adv. Struct. Eng.* **2021**, *24*, 2185–2200. [CrossRef]
12. Bao, X.; Yu, Y.; Liu, C.; Zhao, D.; Chen, X.; Cui, H. Interaction mechanism and influencing factors of multiple structures in deep underground spaces under earthquakes. *J. Build. Struct.* **2023**, *44* (Suppl. S2), 341–349. (In Chinese)
13. Li, M.; An, J.-H.; Zhang, X.-H.; Yue, H.; Zhao, Z. Mode Decomposition Method-reaction Acceleration Method for Seismic Analysis of Metro Station Structure with Large Chassis of Upper Frame Building. *Sci. Technol. Eng.* **2023**, *23*, 3403–3413. (In Chinese)
14. Han, X.; Tao, L.; Zhang, Y.; Jia, Z. A comparative study on the shaking table test of a superstructure subway station structure. *J. Vib. Shock.* **2021**, *40*, 65–74. (In Chinese)
15. Han, X.; Tao, L.; Zhang, Y. Seismic damage mechanism of integrated station structure of urban rail transit hub. *J. Cent. South Univ. (Sci. Technol.)* **2021**, *52*, 925–935. (In Chinese)
16. Li, Y.; Ye, T.; Zong, J. Shaking Table Test on Seismic Response of Tunnel-Soil Surface Structure System considering Soil-Structure Interaction. *Shock. Vib.* **2022**, *2022*, 7515830. [CrossRef]
17. Yao, A.; Tian, T.; Gong, Y.; Li, H. Shaking Table Tests of Seismic Response of Multi-Segment Utility Tunnels in a Layered Liquefiable Site. *Sustainability* **2023**, *15*, 6030. [CrossRef]
18. Ming, S.; Tao, L.; Wang, Z. Shaking Table Testing of Liquefied Soil Layer Located in the Bottom Slab of a Subway Station. *Appl. Sci.* **2023**, *13*, 10866. [CrossRef]
19. Tao, L.; Ding, P.; Yang, X.; Lin, P.; Shi, C.; Bao, Y.; Wei, P.; Zhao, J. Comparative study of the seismic performance of prefabricated and cast-in-place subway station structures by shaking table test. *Tunn. Undergr. Space Technol.* **2020**, *105*, 103583. [CrossRef]
20. Tao, L.; Shi, C.; Ding, P.; Yang, X.; Bao, Y.; Wang, Z. Shaking table test of the effect of an enclosure structure on the seismic performance of a prefabricated subway station. *Tunn. Undergr. Space Technol.* **2022**, *125*, 104533. [CrossRef]
21. Chen, Q.; Zhang, T.; Hong, N.; Huang, B. Seismic Performance of a Subway Station-Tunnel Junction Structure: A Shaking Table Investigation and Numerical Analysis. *KSCE J. Civ. Eng.* **2021**, *25*, 1653–1669. [CrossRef]
22. Zhang, Z.; Yuan, Y.; Li, C.; Yu, H.; Chen, H.; Bilotta, E. Comparison of seismic responses of atrium-style and frame-box metro stations in soft soil in shaking table testing. *Structures* **2022**, *45*, 912–931. [CrossRef]
23. Grasso, S.; Lentini, V.; Sammito, M.S.V. A New Biaxial Laminar Shear Box for 1g Shaking Table Tests on Liquefiable Soils. In Proceedings of the 4th International Conference on Performance Based Design in Earthquake Geotechnical Engineering, Beijing, China, 15–17 July 2022; Volume 52.
24. Buckingham, E. On Physically Similar Systems; Illustrations of the Use of Dimensional Equations. *Phys. Rev. B* **1914**, *4*, 345–376. [CrossRef]

25. Mingzhu, G.; Xudong, C.; Jinyan, Z. Design method of frequency similarity relation for shaking table model test. *Front. Earth Sci.* **2023**, *11*, 1126725.
26. Yang, Z.J.; Su, X.T.; Chen, J.F.; Liu, G.H. Monte Carlo simulation of complex cohesive fracture in random heterogeneous quasi-brittle materials. *Int. J. Solids Struct.* **2009**, *46*, 3222–3234. [CrossRef]